

A Neural-Network Variational Quantum Algorithm for Many-Body Dynamics

Chee Kong Lee,^{1,*} Pranay Patil,² Shengyu Zhang,³ and Chang Yu Hsieh³

¹Tencent America, Palo Alto, CA 94306, United States

²Laboratoire de Physique Théorique, IRSAMC, Université de Toulouse, CNRS, UPS, France

³Tencent Quantum Lab, Shenzhen, Guangdong 518057, China

We propose a neural-network variational quantum algorithm to simulate the time evolution of quantum many-body systems. Based on a modified restricted Boltzmann machine (RBM) wavefunction ansatz, the proposed algorithm can be efficiently implemented in near-term quantum computers with low measurement cost without suffering from the vanishing gradient (or ‘barren plateau’) issue. Using a qubit recycling strategy, only one ancilla qubit is required to represent all the hidden spins in an RBM architecture. The variational algorithm is extended to open quantum systems by employing a stochastic Schrödinger equation approach. Numerical simulations of spin-lattice models demonstrate that our algorithm is capable of capturing the dynamics of closed and open quantum many-body systems with high accuracy.

Accurate and efficient simulation of quantum many-body dynamics remains one of the most challenging problems in physics, despite nearly a century of progress. Renewed interest has been sparked in this field due to recent experiments with Rydberg atoms[1, 2], which suggest the existence of scar states which do not thermalize. This has led to new studies of fragmented Hilbert spaces for such constrained models[3–5], along with further studies on fractons, which are restricted excitations which can disperse only in certain directions[6, 7]. These studies also tie in to the more established field of many body localization[8–10], which studies the possibility of extremely slow relaxation of high energy states in systems with strong disorder. As many of the above phenomena are hard to study analytically, there is a strong motivation to develop powerful numerical tools to further our understanding.

One of the most powerful numerical tools at the disposal of condensed matter theorists is quantum Monte Carlo, which has performed remarkably well for equilibrium physics of numerous systems[11, 12]. This has made important the applicability of this technique to study real time dynamics. This is often impossible due to the infamous sign problem[13, 14], and the one of the few promising ways in which practitioners have attempted to avoid this is by transferring the real time behavior to functions which form coefficients in the wavefunction. These functions then need to have a variational form which can be optimised to get reasonably good results on small systems[15, 16]. Even though one can get around the sign problem for these cases, severe ergodicity restrictions in the Monte Carlo updates may render them inefficient, and necessitate specialized algorithms[17–19]. To allow variational wavefunctions a higher degree of expressibility, some ideas from machine learning, such as restricted Boltzmann machines (RBM), have been used[20–26] to serve as a representation. This has led to a well-controlled way of approximating complicated wavefunctions with rich spatial features. Neural networks have also been used to simulate open quantum systems, which

are numerically more challenging to study than closed systems, and promising results have been achieved for both dynamical[27] and steady state[21, 28, 29] features.

Due to recent advances in quantum computing, it has become possible to program a small number of qubits to directly represent a quantum system using Noisy Intermediate-Scale Quantum (NISQ) technology[30, 31]. One of the many applications of this set up is to speed up the optimization step for variational wavefunctions[32–37]. This serves as a substantial improvement for cases where variational Monte Carlo is inefficient. Direct variational optimization of the time-dependent Schrödinger equation[38–40] has also shown promise, and a large number of general processes can be mapped on to this technique[41].

In this letter, we engineer a neural-network variational quantum algorithm to simulate the dynamics of quantum many-body systems. The algorithm integrates the power of an RBM representation of quantum states with a quantum speed-up coming from transferring the computationally heavy step of calculating expectation values on to the quantum computer. We show that the variational algorithm can be extended to the dynamics of open quantum systems using a stochastic Schrödinger equation approach. The proposed method is benchmarked against canonical spin-lattice models and performs well for dynamics of both closed and open systems.

Neural Network Quantum States: An RBM quantum state can be obtained from a bipartite Ising Hamiltonian

$$\hat{H}_{RBM}(\theta) = \sum_i b_i \hat{v}_i^z + \sum_j m_j \hat{h}_j^z + \sum_{ij} W_{ij} \hat{v}_i^z \hat{h}_j^z, \quad (1)$$

where \hat{v}_i^z or \hat{h}_j^z is the Pauli-Z operator for the visible or hidden qubit, respectively. We denote the complex-valued variational RBM parameters as $\theta = [b, m, W]$. To prepare a complex-valued RBM state [42], we first entangle $N + M$ qubits (representing N visible and M hidden spins of an RBM architecture) according to

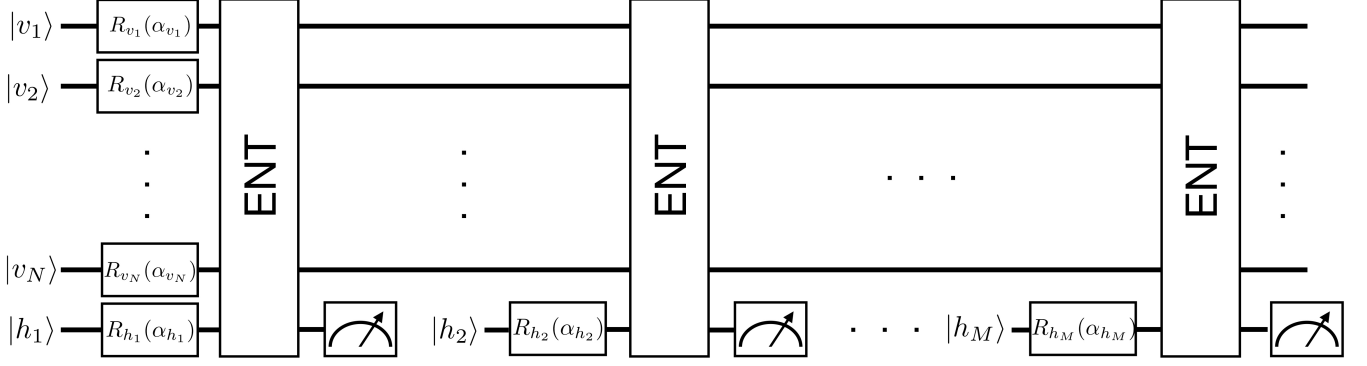


FIG. 1. Quantum circuit for preparing uRBM state with qubit recycling scheme described in Eq. 4. All the qubits are initialized in $|0\rangle$ state. The single rotations are governed by the relations in Eq. 5. The j -th entangling block implements the $\exp(i \sum_i W_{ij}^I \hat{v}_i^z \hat{h}_j^z)$ operator and its explicit form is given in the Supplemental Material. After each entangling block, the ancilla qubit representing the j -th hidden spin is projected onto $|+\rangle$ state before being recycled.

$$|\Psi_{vh}(\theta)\rangle = \frac{e^{\hat{H}_{RBM}(\theta)}}{N_{vh}} |++\dots+\rangle_{vh}, \quad (2)$$

where $|+\rangle = \frac{1}{\sqrt{2}}(|0\rangle + |1\rangle)$, $N_{vh} = \sqrt{\langle ++\dots+ | e^{2\hat{H}_{RBM}^R(\theta)} | ++\dots+\rangle_{vh}}$, $\hat{H}_{RBM}^R(\theta)$ is the Hermitian part of the RBM Hamiltonian and the subscript vh denotes visible and hidden (ancilla) qubits. Eq. 2 gives a conceptually simple wave function that could be generated by first applying single-qubit transformations $\exp(b_i \hat{v}_i^z)$ and $\exp(m_j \hat{h}_j^z)$ on individual qubits followed by $\exp(W_{ij} \hat{v}_i^z \hat{h}_j^z)$ to couple the visible and hidden qubits.

Once the extended wave function $|\Psi_{vh}(\theta)\rangle$ is generated, all ancilla qubits (i.e. hidden spins) are post-selected for $|+\rangle_h$ and the desired RBM state is implemented in a quantum circuit

$$|\Psi_v(\theta)\rangle = \frac{\langle ++\dots+ | \Psi_{vh}(\theta)\rangle}{N_v}, \quad (3)$$

where $N_v = \sqrt{\langle \Psi_{vh}(\theta) | \hat{P}_+^{(h)} | \Psi_{vh}(\theta)\rangle}$ and $\hat{P}_+^{(h)} = |++\dots+\rangle_h \langle ++\dots+|$ projects all the hidden spins onto $|+\rangle$ state.

Observing that Eq. 3 can be cast in the following form:

$$\begin{aligned} |\Psi_v(\theta)\rangle &= \frac{1}{N_v} \left[\langle + | \left[e^{\hat{h}_M^z (m_M + \sum_i W_{iM} \hat{v}_i^z)} \right] | + \rangle \right]_M (4) \\ &\times \left[\langle + | \left[e^{\hat{h}_{M-1}^z (m_{M-1} + \sum_i W_{iM-1} \hat{v}_i^z)} \right] | + \rangle \right]_{M-1} \dots \\ &\left[\langle + | \left[e^{\hat{h}_1^z (m_1 + \sum_i W_{i1} \hat{v}_i^z)} \right] | + \rangle \right]_1 e^{\sum_i b_i \hat{v}_i^z} | ++\dots+\rangle_v, \end{aligned}$$

where $[\langle + | [\dots] | + \rangle]_j$ encodes the effect of j -th hidden spin on all visible spins, it is clear a single ancilla qubit is sufficient to implement the entangling operation sequentially.

The above quantum operations are non-unitary when RBM parameters are complex, i.e. $b_i^R \neq 0$, $m_j^R \neq 0$ or $W_{ij}^R \neq 0$, where we use superscripts R and I to denote the real and imaginary parts of the RBM parameters. In particular, the non-unitary two-qubit operation mediating entanglement across the visible-hidden layer are difficult to implement. One could adopt a probabilistic scheme [43] to generate the inter-layer couplings with an extra ancilla qubit. However, for complex-valued wavefunction, this approach is difficult to scale with the number of qubits involved due to low success probability.

For this reason, we only consider the unitary-coupled RBM (uRBM) ansatz in which $W_{ij}^R = 0$ for the rest of this letter [42]. Fig. 1 depicts a quantum circuit for preparing a uRBM state composed of N visible spins and M hidden spins. After initializing all qubits in $|0\rangle$ state, we first perform single qubit rotations representing the terms $\exp(b_i \hat{v}_i^z)$ and $\exp(m_j \hat{h}_j^z)$. The rotation angles, α_{v_i/h_j} , are governed by the relations

$$\begin{aligned} R_{v_i}(\alpha_{v_i})|0\rangle &= e^{b_i \hat{v}_i^z} |+\rangle / c_{v_i}, \quad (5) \\ R_{h_j}(\alpha_{h_j})|0\rangle &= e^{m_j \hat{h}_j^z} |+\rangle / c_{h_j}, \end{aligned}$$

where the normalization factors are $c_{v_i} = \sqrt{\langle + | \exp(2b_i \hat{v}_i^z) | + \rangle}$ and $c_{h_j} = \sqrt{\langle + | \exp(2m_j \hat{h}_j^z) | + \rangle}$.

The j -th entangling block implements the coupling term $\exp(i \sum_i W_{ij}^I \hat{v}_i^z \hat{h}_j^z)$ and are composed of a series of controlled-Z rotations. The details of the entangling block are given in the Supplemental Material (SM). Employing the qubit recycling scheme described in Eq. 4, the ancilla qubit representing the j -th hidden spin is projected onto $|+\rangle$ state after each entangling block before being recycled. Thus we only need $N + 1$ qubits in total, and the number of quantum gates is proportional to the number of variational parameters, N_{var} , which scales as $O(\alpha N^2)$ where $\alpha = N/M$.

Time-dependent Variational Algorithm: We adopt a hybrid quantum-classical approach based on the time-dependent variational Monte Carlo (t-VMC) method to simulate the quantum dynamics [44–46]. In t-VMC framework, we minimize the residue in $\min_{\theta} \|\hat{1} \frac{\partial |\Psi(\theta)\rangle}{\partial t} - \hat{H}_s |\Psi(\theta)\rangle\|$, where \hat{H}_s is the system Hamiltonian and the norm is defined as the square root of the inner product. The resulting equations of motion for the time-dependent variational parameters are

$$\dot{\theta}_n = \sum_m A_{nm}^{-1} \text{Im}[f_m]. \quad (6)$$

The covariance matrix A and force vector f read

$$A_{nm} = \text{Re}\langle \hat{O}_n^\dagger \hat{O}_m \rangle_v - \text{Re}\langle \hat{O}_n^\dagger \rangle_v \text{Re}\langle \hat{O}_m \rangle_v, \quad (7)$$

$$f_m = \langle \hat{O}_m^\dagger \hat{H}_s \rangle_v - \text{Re}\langle \hat{O}_m^\dagger \rangle_v \langle \hat{H}_s \rangle_v, \quad (8)$$

where $\langle \cdots \rangle_v = \langle \Psi_v(\theta) | \cdots | \Psi_v(\theta) \rangle$. The derivative operators with respect to the n -th variational parameter is defined as $\hat{O}_n = \frac{\partial \ln |\Psi_v(\theta)\rangle}{\partial \theta_n}$. For RBM state defined in Eq. 3, the \hat{O}_n operators can be derived analytically which allows an efficient way of obtaining the gradients

$$\hat{O}_n = \begin{cases} i^{1-\delta} \hat{v}_i^z, & \text{if } \theta_n = b_i, \\ i^{1-\delta} \tanh(m_j + \sum_i W_{ij} \hat{v}_i^z), & \text{if } \theta_n = m_j, \\ i \hat{v}_i^z \tanh(m_j + \sum_i W_{ij} \hat{v}_i^z), & \text{if } \theta_n = W_{ij}, \end{cases} \quad (9)$$

where $\delta = 0$ if $\theta_n = b_i^I$ or $\theta_n = m_j^I$ or $\theta_n = W_{ij}^I$, and $\delta = 1$ if $\theta_n = b_i^R$ or $\theta_n = m_j^R$. The variational parameters are updated iteratively according to $\theta_n(t + \delta t) = \theta_n(t) + A^{-1} \text{Im}[f] \delta t$ where δt is the update time step.

In conventional t-VMC, the covariance matrix A and force vector f in Eq. 7 are obtained from Markov chain random walk approach, such as the Metropolis-Hastings algorithm. Such sampling could be challenging for systems that exhibit long correlation time, e.g. systems near phase transition. In a hybrid quantum-classical framework, both A and f are sampled directly from the output of quantum circuit depicted in Fig. 1, circumventing the difficulties associated with Markov chain methods.

Simulation Results: To demonstrate the performance of the uRBM algorithm in simulating many-body quantum dynamics, we first consider a 1D transverse-field Ising (TFI) model:

$$\hat{H}_{TFI} = -h \sum_i \hat{\sigma}_i^x - \sum_{\langle ij \rangle} \hat{\sigma}_i^z \hat{\sigma}_j^z, \quad (10)$$

where h denotes the strength of the transverse field. Here we study the dynamics of a TFI model induced by quantum quench. The TFI system is initially prepared in the ground state for an initial transverse field h_i . The variational parameters of the initial ground state wavefunction are obtained using a hybrid imaginary time algorithm [42], the details can be found in SM. At $t = 0$, we introduce an instantaneous change to the transverse field, $h_f \neq h_i$, and let the system evolves under the new Hamiltonian.

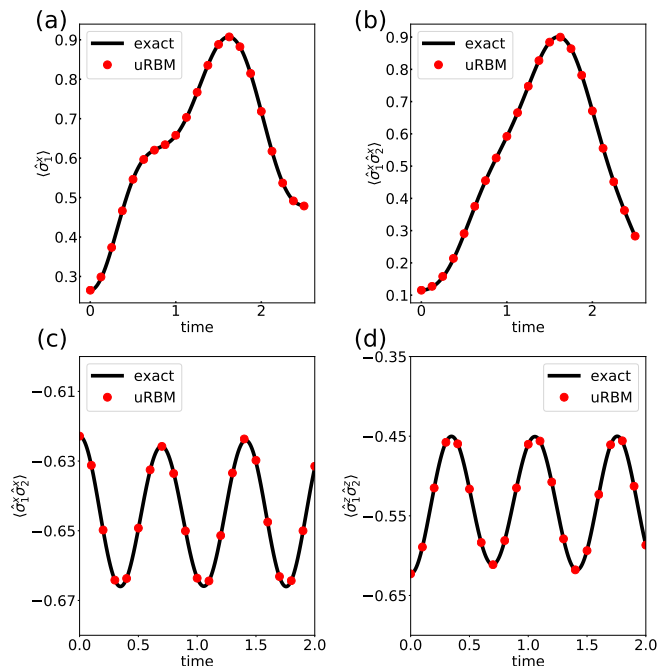


FIG. 2. Time evolution induced by quantum quench. Results from uRBM algorithm (symbols) are compared to exact calculations (solids lines). (a) and (b) Dynamics of transverse polarization and its correlation in a 1D Ising model. (c) and (d) Dynamics of magnetization and transverse polarization correlations in a 1D Heisenberg model.

In Fig. 2 (a) and (b), we consider a TFI model of 6 spins with periodic boundary condition and the transverse field is changed from $h_i = 0.5$ to the critical value of $h_f = 1.0$ at $t = 0$. In the simulations we use $\delta t = 0.0005$ and $\alpha = M/N = 4$. We compare the results from the uRBM algorithm with results from exact diagonalization by studying the evolution of transverse spin polarization $\langle \sigma_1^x \rangle$ and its correlation $\langle \sigma_1^x \sigma_2^x \rangle$. The good agreement with exact results confirms the accuracy of the uRBM algorithm in capturing quantum many-body dynamics.

Next we consider a 1D anisotropic Heisenberg model with periodic boundary condition in a magnetic field:

$$\hat{H}_H = -h_z \sum_i \hat{\sigma}_i^z + \sum_{\langle ij \rangle} (J_z \hat{\sigma}_i^z \hat{\sigma}_j^z + \hat{\sigma}_i^x \hat{\sigma}_j^x + \hat{\sigma}_i^y \hat{\sigma}_j^y) \quad (11)$$

where h_z is the strength of longitudinal field and J_z is the longitudinal coupling. Again we perform a quantum quench by instantaneously changing the longitudinal coupling from $J_z = 1.0$ to $J_z = 0.5$ at $t = 0$. Figs. 2 (c) and (d) depict the dynamics of spin-spin correlations of a 6-spin Heisenberg model with $h_z = 1.0$. We use $\delta t = 0.0002$ and $\alpha = 6$ in our simulations. Again we observe near exact agreement between the results from the uRBM algorithm and exact diagonalization, further confirming the capability of the hybrid uRBM algorithm.

Open Quantum Systems: Extending the variational

uRBM algorithm to open quantum systems is conceptually straight forward using the stochastic wavefunction approach. The dynamics of the density matrix, $\hat{\rho}$, of an open quantum system can be described by the Lindblad master equation [47]

$$\frac{d\hat{\rho}}{dt} = -i[\hat{H}_s, \hat{\rho}] + \frac{1}{2} \sum_k [2\hat{L}_k \hat{\rho} \hat{L}_k^\dagger - \{\hat{L}_k^\dagger \hat{L}_k, \hat{\rho}\}], \quad (12)$$

where $\{\cdot\}$ denotes an anti-commutator, \hat{H}_s is the system Hamiltonian and the Lindblad operators \hat{L}_k describe the interaction between the system and a Markovian bath. Instead of solving the Lindblad master equation directly, an open quantum system can be equivalently described by an ensemble of pure state trajectories [48, 49]. The evolution of these pure state trajectories is governed by a non-Hermitian effective Hamiltonian $\hat{H}_{eff} = \hat{H}_s - \frac{i}{2} \sum_k (\hat{L}_k \hat{L}_k^\dagger - \langle \hat{L}_k \hat{L}_k^\dagger \rangle)$ and subject to continuous measurement. The details of implementing these stochastic wavefunction trajectories in quantum circuits can be found in SM.

We test the ability of the hybrid uRBM algorithm in simulating the dynamics of an open quantum system by considering a 4-spin 1D TFI model with open boundary condition coupled to a Markovian bath. All the spins of the TFI model are initially prepared in $|+\rangle = \frac{1}{\sqrt{2}}(|0\rangle + |1\rangle)$ state. The Lindblad operator is $\hat{L}_k = \sqrt{\gamma} \hat{\sigma}_k^+$ where $\hat{\sigma}_k^+$ is a raising operator acting on the k -th spin and γ determines the strength of system-bath interaction. Other parameters used in the simulation are $\alpha = M/N = 6$, $\gamma = 0.2$, $h = 1.0$, $\delta t = 0.0005$. The dynamics of transverse polarization and its correlation are compared to those from directly solving Eq. 12. It can be seen that the uRBM algorithm is capable of simulating the dynamics of open systems with high accuracy. This further extend the applicability to the hybrid uRBM algorithm to study novel non-equilibrium phenomena in many-body open quantum systems such as phase transitions [50, 51].

Discussions: The proposed hybrid uRBM algorithm offers several advantages compared to other NISQ variational algorithms. First our numerical results (see SM) show that the gradients in the uRBM ansatz do not decay exponentially with system size, indicating the absence of the vanishing gradient (or ‘barren plateau’) issue that affects many variational quantum algorithms [52]. In fact, classical implementations of VMC using RBM ansatz has been demonstrated on systems with more than 100 visible spins [53] using the covariance matrix and force vector defined in Eq. 7.

Second, real and imaginary time variational algorithms [38, 39, 41, 54] typically require significantly more measurements (and distinct quantum circuits) than gradient descent approaches such as variational quantum eigensolver (VQE) due of the estimation of covariance matrix A . The number of matrix elements in A scales as $O(N_{var}^2)$

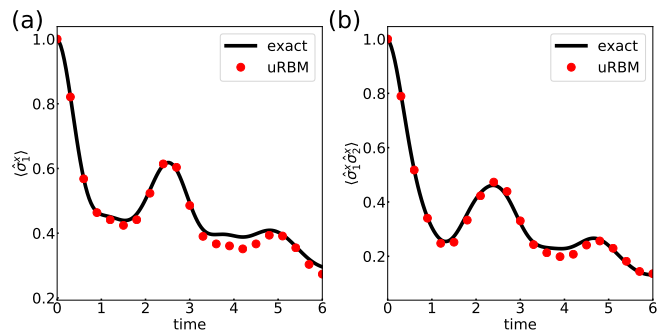


FIG. 3. Dynamics of a dissipative 1D Ising model obtained from exact numerical solution of Eq.12 (solid lines) and from the hybrid uRBM algorithm (symbols). The simulation results from the hybrid uRBM algorithm are obtained from averaging over 2000 pure state trajectories.

where N_{var} is the number of variational parameters. This measurement cost could be prohibitive in large scale simulation in NISQ devices since N_{var} will be a big number. Within RBM ansatz all the matrix elements in A can be expressed analytically in terms of the Pauli-Z operators of the visible spins (see Eq. 9), a single measurement in the Z-basis contributes to the statistics of all the matrix elements in A , thus significantly reducing the number of measurements and distinct circuits required.

Additionally, the uRBM algorithm offers great flexibility when it comes to the number of ancilla qubits (for hidden spins) and circuit depth. Employing the qubit recycling scheme depicted in Fig.1, we only need $N + 1$ total number of qubits but a circuit depth of $O(\alpha N^2)$ to implement the uRBM state. At the opposite end of the spectrum, we could use M ancilla qubits to represent M hidden spins, this reduces the circuit depth to $O(N)$, assuming full connectivity like those found in ion-trap based quantum computers [55, 56]. Of course, one could envision an optimal trade-off between qubit number and circuit depth that takes the architecture of the hardware into account.

Finally, the accuracy of the uRBM algorithm can be systematically improved by including more hidden spins. For quantum systems that are very strongly correlated, our method can be extended to deep Boltzmann machines (DBM) in a straight forward manner. DBM contains more than one layer of hidden spins and has been shown to be able to efficiently represent most quantum states generated by quantum dynamics [57, 58].

Conclusions: We have introduced a neural-network based variational quantum algorithm to simulate the dynamics of closed and open quantum many-body systems. Our results show that the proposed algorithm is capable of capturing the dynamics of both types of systems with high accuracy. A key benefit that the integration of quantum devices provides over traditional variational quantum Monte Carlo is the elimination of the sign problem

and ergodicity issues. Additionally, the proposed variational algorithm offers several advantages over existing NISQ approaches, including absence of barren plateaus, flexibility in qubit-number versus circuit-depth trade-off and low measurement cost. These advantages make the algorithm particularly appealing for implementation in NISQ devices.

Note: During the preparation of this manuscript, we became aware of related works based on deep quantum feedforward neural networks [59] and matrix product states [60].

* cheekonglee@tencent.com

- [1] H. Bernien, S. Schwartz, A. Keesling, H. Levine, A. Omran, H. Pichler, S. Choi, A. S. Zibrov, M. Endres, M. Greiner, *et al.*, *Nature* **551**, 579 (2017).
- [2] A. Celi, B. Vermersch, O. Viyuela, H. Pichler, M. D. Lukin, and P. Zoller, *Physical Review X* **10**, 021057 (2020).
- [3] P. Sala, T. Rakovszky, R. Verresen, M. Knap, and F. Pollmann, *Physical Review X* **10**, 011047 (2020).
- [4] Z.-C. Yang, F. Liu, A. V. Gorshkov, and T. Iadecola, *Physical Review Letters* **124**, 207602 (2020).
- [5] G. De Tomasi, D. Hetterich, P. Sala, and F. Pollmann, *Physical Review B* **100**, 214313 (2019).
- [6] R. M. Nandkishore and M. Hermele, *Annual Review of Condensed Matter Physics* **10**, 295 (2019).
- [7] C. Chamon, *Physical review letters* **94**, 040402 (2005).
- [8] F. Alet and N. Laflorencie, *Comptes Rendus Physique* **19**, 498 (2018).
- [9] A. Pal and D. A. Huse, *Physical review b* **82**, 174411 (2010).
- [10] R. Nandkishore and D. A. Huse, *Annu. Rev. Condens. Matter Phys.* **6**, 15 (2015).
- [11] M. Suzuki, *Quantum Monte Carlo methods in condensed matter physics* (World scientific, 1993).
- [12] D. Ceperley and B. Alder, *Science* **231**, 555 (1986).
- [13] R. Bishop and D. J. Farnell, in *Recent Progress In Many-Body Theories* (World Scientific, 2000) pp. 457–460.
- [14] M. Troyer and U.-J. Wiese, *Physical review letters* **94**, 170201 (2005).
- [15] G. Carleo, L. Cevolani, L. Sanchez-Palencia, and M. Holzmann, *Physical Review X* **7**, 031026 (2017).
- [16] K. Ido, T. Ohgoe, and M. Imada, *Physical Review B* **92**, 245106 (2015).
- [17] S. Biswas, G. Rakala, and K. Damle, *Physical Review B* **93**, 235103 (2016).
- [18] O. F. Syljuåsen and A. W. Sandvik, *Physical Review E* **66**, 046701 (2002).
- [19] Z. Yan, Y. Wu, C. Liu, O. F. Syljuåsen, J. Lou, and Y. Chen, *Physical Review B* **99**, 165135 (2019).
- [20] G. Carleo and M. Troyer, *Science* **355**, 602 (2017).
- [21] A. Nagy and V. Savona, *Phys. Rev. Lett.* **122**, 250501 (2019).
- [22] I. Glasser, N. Pancotti, M. August, I. D. Rodriguez, and J. I. Cirac, *Phys. Rev. X* **8**, 11006 (2018).
- [23] M. Schmitt and M. Heyl, *Physical Review Letters* **125**, 100503 (2019).
- [24] I. L. Gutiérrez and C. B. Mendl, (2019), arXiv:1912.08831.
- [25] D.-L. Deng, X. Li, and S. D. Sarma, *Phys. Rev. B* **96**, 195145 (2017).
- [26] S. D. Sarma, D.-L. Deng, and L.-M. Duan, *Physics Today* **72**, 48 (2019).
- [27] M. J. Hartmann and G. Carleo, *Physical Review Letters* **122**, 250502 (2019), arXiv:1902.05131.
- [28] F. Vicentini, A. Biella, N. Regnault, and C. Ciuti, *Physical review letters* **122**, 250503 (2019).
- [29] N. Yoshioka and R. Hamazaki, *Phys. Rev. B* **99**, 214306 (2019).
- [30] J. Preskill, *Quantum* **2**, 79 (2018).
- [31] F. Arute, K. Arya, R. Babbush, D. Bacon, J. C. Bardin, R. Barends, R. Biswas, S. Boixo, F. G. S. L. Brandao, D. A. Buell, B. Burkett, Y. Chen, Z. Chen, B. Chiaro, R. Collins, W. Courtney, A. Dunsworth, E. Farhi, B. Foxen, A. Fowler, C. Gidney, M. Giustina, R. Graff, K. Guerin, S. Habegger, M. P. Harrigan, M. J. Hartmann, A. Ho, M. Hoffmann, T. Huang, T. S. Humble, S. V. Isakov, E. Jeffrey, Z. Jiang, D. Kafri, K. Kechedzhi, J. Kelly, P. V. Klimov, S. Knysh, A. Korotkov, F. Kostritsa, D. Landhuis, M. Lindmark, E. Lucero, D. Lyakh, S. Mandrà, J. R. McClean, M. McEwen, A. Megrant, X. Mi, K. Michielsen, M. Mohseni, J. Mutus, O. Naaman, M. Neeley, C. Neill, M. Y. Niu, E. Ostby, A. Petukhov, J. C. Platt, C. Quintana, E. G. Rieffel, P. Roushan, N. C. Rubin, D. Sank, K. J. Satzinger, V. Smelyanskiy, K. J. Sung, M. D. Trevithick, A. Vainsencher, B. Villalonga, T. White, Z. J. Yao, P. Yeh, A. Zalcman, H. Neven, and J. M. Martinis, *Nature* **574**, 505 (2019).
- [32] J. R. McClean, J. Romero, R. Babbush, and A. Aspuru-Guzik, *New Journal of Physics* **18** (2016), 10.1088/1367-2630/18/2/023023, arXiv:1509.04279.
- [33] A. Peruzzo, J. McClean, P. Shadbolt, M.-H. Yung, X.-Q. Zhou, P. J. Love, A. Aspuru-Guzik, and J. L. O’Brien, *Nature Communications* **5**, 4213 (2014), arXiv:1304.3061.
- [34] E. Farhi, J. Goldstone, and S. Gutmann, arXiv preprint arXiv:1411.4028 (2014).
- [35] A. Kandala, A. Mezzacapo, K. Temme, M. Takita, M. Brink, J. M. Chow, and J. M. Gambetta, *Nature* **549**, 242 (2017).
- [36] C. Hempel, C. Maier, J. Romero, J. McClean, T. Monz, H. Shen, P. Jurcevic, B. P. Lanyon, P. Love, R. Babbush, and Others, *Phys. Rev. X* **8**, 31022 (2018).
- [37] J. I. Colless, V. V. Ramasesh, D. Dahlen, M. S. Blok, M. E. Kimchi-Schwartz, J. R. McClean, J. Carter, W. A. De Jong, and I. Siddiqi, *Phys. Rev. X* **8**, 11021 (2018).
- [38] Y. Li and S. C. Benjamin, *Physical Review X* **7**, 021050 (2017).
- [39] X. Yuan, S. Endo, Q. Zhao, Y. Li, and S. C. Benjamin, *Quantum* **3**, 191 (2019).
- [40] K. Heya, K. M. Nakanishi, K. Mitarai, and K. Fujii, (2019), arXiv:1904.08566.
- [41] S. Endo, J. Sun, Y. Li, S. C. Benjamin, and X. Yuan, *Physical Review Letters* **125**, 010501 (2020), arXiv:1812.08778.
- [42] C.-y. Hsieh, Q. Sun, S. Zhang, and C. K. Lee, (2019), arXiv:1912.02988.
- [43] R. Xia and S. Kais, *Nat. Commun.* **9**, 4195 (2018).
- [44] G. Carleo, F. Becca, M. Schiró, and M. Fabrizio, *Scientific Reports* **2**, 243 (2012).
- [45] G. Carleo, F. Becca, L. Sanchez-Palencia, S. Sorella, and

- M. Fabrizio, *Physical Review A* **89**, 031602 (2014).
- [46] F. Becca and S. Sorella, *Quantum Monte Carlo Approaches for Correlated Systems* (Cambridge University Press, 2017).
- [47] H.-P. Breuer and F. Petruccione, *The Theory of Open Quantum Systems* (Oxford University Press, 2007).
- [48] J. Dalibard, Y. Castin, and K. Mølmer, *Physical Review Letters* **68**, 580 (1992).
- [49] H. J. Carmichael, *Physical Review Letters* **70**, 2273 (1993).
- [50] T. Fink, A. Schade, S. Höfling, C. Schneider, and A. Imamoglu, *Nature Physics* **14**, 365 (2018).
- [51] J. Raftery, D. Sadri, S. Schmidt, H. E. Türeci, and A. A. Houck, *Physical Review X* **4**, 031043 (2014).
- [52] J. R. McClean, S. Boixo, V. N. Smelyanskiy, R. Babbush, and H. Neven, *Nature communications* **9**, 4812 (2018).
- [53] R. Zen, L. My, R. Tan, F. Hébert, M. Gattobigio, C. Miniatura, D. Poletti, and S. Bressan, *Physical Review E* **101**, 053301 (2020).
- [54] S. McArdle, T. Jones, S. Endo, Y. Li, S. C. Benjamin, and X. Yuan, *npj Quantum Information* **5** (2019).
- [55] K. R. Brown, J. Kim, and C. Monroe, *npj Quantum Inf.* **2**, 16034 (2016).
- [56] C. D. Bruzewicz, J. Chiaverini, R. McConnell, and J. M. Sage, *Appl. Phys. Rev.* **6**, 21314 (2019).
- [57] X. Gao and L. M. Duan, *Nature Communications* **8**, 1 (2017), arXiv:1701.05039.
- [58] G. Carleo, Y. Nomura, and M. Imada, *Nat. Commun.* **9**, 5322 (2018).
- [59] Z. Liu, L. M. Duan, and D.-L. Deng, (2020), arXiv:2008.05488.
- [60] S.-H. Lin, R. Dilip, A. G. Green, A. Smith, and F. Pollmann, , 1 (2020), arXiv:2008.10322.

Supplemental Material: A Neural-Network Variational Quantum Algorithm for Many-Body Dynamics

Chee Kong Lee,^{1,*} Pranay Patil,² Shengyu Zhang,³ and Chang Yu Hsieh³

¹Tencent America, Palo Alto, CA 94306, United States

²Laboratoire de Physique Théorique, IRSAMC, Université de Toulouse, CNRS, UPS, France

³Tencent Quantum Lab, Shenzhen, Guangdong 518057, China

Implementation of the entangling gates

For unitary coupled RBM (uRBM) ansatz ($W_{ij}^R = 0$), the j -th entangling block in the quantum circuit of Fig. 1 in the main text implements the operation $\exp(i \sum_i W_{ij}^I \hat{v}_i^z \hat{h}_j^z)$ that couples the j -th hidden spin with all the visible spins. The quantum circuit for each coupling term $\exp(iW_{ij}^I \hat{v}_i^z \hat{h}_j^z)$ is shown in Fig.S1(a) where $\theta_{ij} = -\theta'_{ij} = -W_{ij}^I$. For full RBM states with complex value couplings, the non-unitary operation $\exp(W_{ij}^R \hat{v}_i^z \hat{h}_j^z)$ can be implemented using the probabilistic scheme introduced by Xia and Sabre [1] to generate the inter-layer couplings with an extra ancilla qubit. The quantum circuit of this scheme is shown in Fig.S1(b). The rotation angles in the controlled gates are

$$\begin{aligned}\theta_{ij,1} &= 2 \sin^{-1}(\sqrt{\exp(W_{ij}^R - |W_{ij}^R|)}), \\ \theta_{ij,2} &= 2 \sin^{-1}(\sqrt{\exp(-W_{ij}^R - |W_{ij}^R|)}).\end{aligned}\tag{1}$$

After each operation $\exp(\sum_i W_{ij}^R \hat{v}_i^z \hat{h}_j^z)$ is implemented, the ancilla qubit is measured. If the ancilla qubit is in state $|1\rangle$, we continue to the next coupling term, otherwise we start from the beginning. Given the $N * M$ number of probabilistic measurements of the ancilla qubit, this approach is difficult to scale with the number of qubits for large scale simulation.

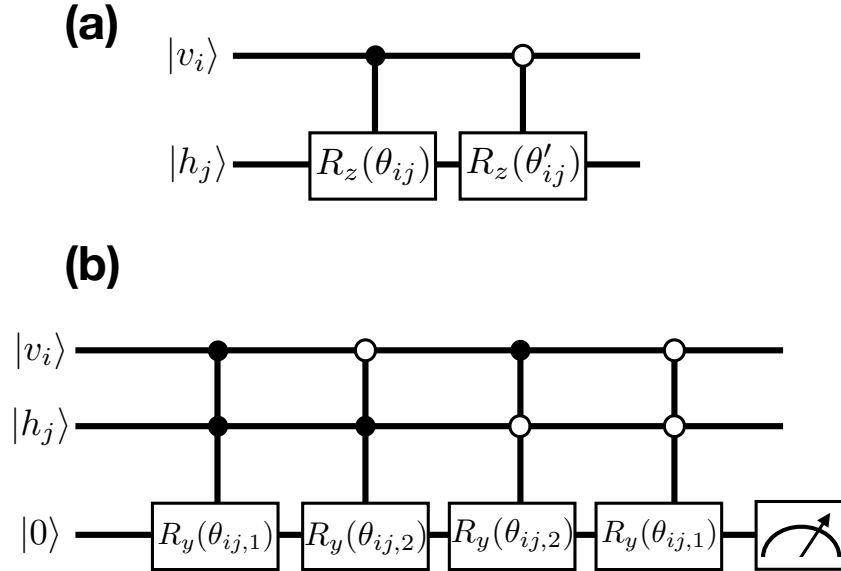


FIG. S1: Quantum circuits for the coupling terms (a) $\exp(i \sum_i W_{ij}^I \hat{v}_i^z \hat{h}_j^z)$ and (b) $\exp(\sum_i W_{ij}^R \hat{v}_i^z \hat{h}_j^z)$ between i -th visible and j -th hidden spins, .

Variational imaginary time evolution

In the numerical examples of closed systems in Fig. 2 of the main text, the initial states are prepared as the ground states of the initial Hamiltonians before quantum quenches. The variational parameters of these initial wavefunctions are obtained via a variational quantum-classical imaginary time evolution (ITE) following the Stochastic Reconfiguration framework [2]. The update rule of the variational parameters in the hybrid ITE algorithm is

$$\dot{\theta}_n(\tau) = \sum_m A_{nm}^{-1} \text{Re}[f_m]. \quad (2)$$

where τ denotes the imaginary time, the definitions of the covariance matrix A and the force vector f are the same as the real time algorithm (i.e. Eqs. (7) and (8)) in the main text. The parameters are updated iteratively

$$\theta_n(\tau + \delta\tau) = \theta_n(\tau) + \delta\tau A^{-1} \text{Re}[f] \quad (3)$$

where $\delta\tau$ is the imaginary time step. In our simulations, we use $\delta\tau = 0.01$ for 2500 steps. At $\tau = 0$, the variational RBM parameters are initialized as Gaussian random numbers with zero mean and variance of 0.01. The imaginary time evolution of the 6-spin 1D Ising and Heisenberg models used in the main text are shown in Fig. S2.

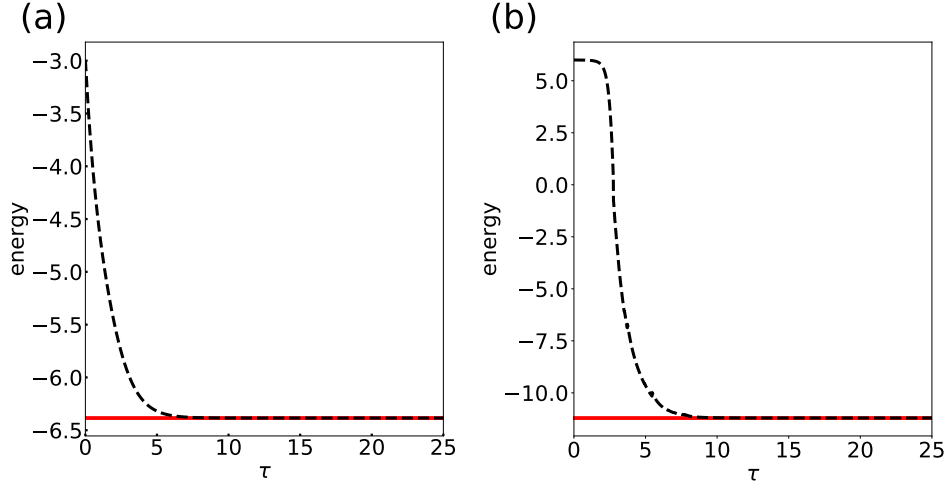


FIG. S2: Imaginary time evolution of (a) 1D Ising model and (b) Heisenberg models. The solid lines are the exact ground-state energy. The dashed black lines represent the imaginary time evolution using the variational uRBM algorithm.

Derivations of wavefunction derivatives

The derivative of $|\Psi_v(\theta)\rangle$ can be written as

$$\left| \frac{\partial \Psi_v}{\partial \theta_n} \right\rangle = \frac{h \langle ++ \dots + | \partial_{\theta_n} \tilde{\Psi}_{vh} \rangle}{\tilde{N}_v} - \text{Re} \left(\frac{\langle \tilde{\Psi}_{vh} | \hat{P}_+^{(h)} | \partial_{\theta_n} \tilde{\Psi}_{vh} \rangle}{\tilde{N}_v} \right) \frac{h \langle ++ \dots + | \tilde{\Psi}_{vh} \rangle}{\tilde{N}_v}, \quad (4)$$

where $|\tilde{\Psi}_{vh}(\theta)\rangle = \sum_{\mathbf{h}} e^{\hat{H}_{RBM}(\theta, \mathbf{h})} |++ \dots +\rangle_v$ is the unnormalized wavefunction and $N_v = \sqrt{\langle \Psi_{vh}(\theta) | P_+^{(h)} | \Psi_{vh}(\theta) \rangle}$. $\hat{H}_{RBM}(\theta, h)$ is the RBM Hamiltonian with the hidden spins \hat{h}_j^z replaced with binary values of ± 1 . The derivatives of $|\tilde{\Psi}_{vh}(\theta)\rangle$ are in turn given by

$$\begin{aligned} \frac{\partial |\tilde{\Psi}_{vh}\rangle}{\partial b_i^R} &= \hat{v}_i^z |\tilde{\Psi}_{vh}\rangle, & \frac{\partial |\tilde{\Psi}_{vh}\rangle}{\partial m_j^R} &= \tanh(m_j + \sum_i W_{ij} \hat{v}_i^z) |\tilde{\Psi}_{vh}\rangle, \\ \frac{\partial |\tilde{\Psi}_{vh}\rangle}{\partial W_{ij}^R} &= \hat{v}_i^z \tanh(m_j + \sum_i W_{ij} \hat{v}_i^z) |\tilde{\Psi}_{vh}\rangle, & \frac{\partial |\tilde{\Psi}_{vh}\rangle}{\partial b_i^I} &= i \hat{v}_i^z |\tilde{\Psi}_{vh}\rangle, \\ \frac{\partial |\tilde{\Psi}_{vh}\rangle}{\partial m_j^I} &= i \tanh(m_j + \sum_i W_{ij} \hat{v}_i^z) |\tilde{\Psi}_{vh}\rangle, & \frac{\partial |\tilde{\Psi}_{vh}\rangle}{\partial W_{ij}^I} &= i \hat{v}_i^z \tanh(m_j + \sum_i W_{ij} \hat{v}_i^z) |\tilde{\Psi}_{vh}\rangle. \end{aligned} \quad (5)$$

Substituting Eqs. 4-5 into in the derivative operator, $O_n = \frac{\partial \ln |\Psi_v\rangle}{\partial \theta_n}$, we arrive at Eq.(9) in the main text.

Gradients of uRBM Parameters

Here we show that the proposed uRBM algorithm does not suffer from the ‘barren plateau’ issue that affects many variational quantum algorithms [3]. In Fig. S3 we plot the norms of the force vector, f , and the gradient, $A^{-1}f$, as a function of system size, both quantities are normalized by the total number of variational parameters. We consider a 1D transverse field Ising model (panels (a) and (b)) and a 1D Heisenberg model in longitudinal field (panels (c) and (d)) with periodic boundary condition, both with magnetic field strength $h = 1.0$. The number of hidden spins is fixed at $M = 6$. The RBM parameters are randomly initialized as Gaussian variables with variance of 0.01, the blue and red lines in Fig. S3 denote the average and minimum of 100 random initializations, respectively.

The force vector, f , is simply the gradient vector of the energy function, $E_\theta = \langle \Psi_v | (\theta) H_s | \Psi_v \rangle (\theta)$, whereas the real and imaginary parts of $A^{-1}f$ dictate the parameter update in imaginary and real time evolution (see Eq. 6 in main text and Eq. 2 above), respectively. From Fig. S3, we can clearly see that both f and $A^{-1}f$ do not decay exponentially with system size, indicating the uRBM algorithm does not suffer from the vanishing gradient (or ‘barren plateau’) issue.

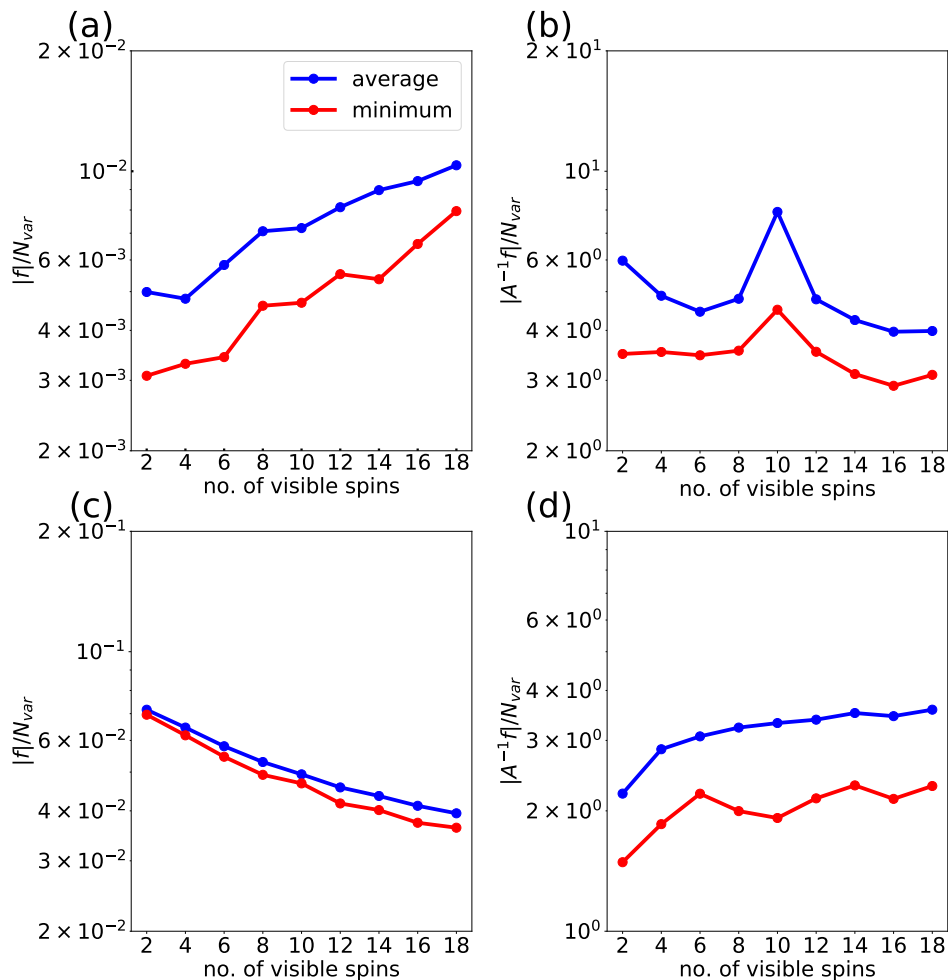


FIG. S3: The norms of f and $A^{-1}f$ as a function of system size for a 1D transverse field Ising model ((a) and (b)) and a 1D Heisenberg model in longitudinal field ((c) and (d)). The norms are normalized by the number of variational parameters. The blue and red lines denote the average and minimum from 100 random initializations, respectively.

Stochastic Schrödinger Equation

The dynamics of an open quantum system coupled to a Markovian bath can be described by an ensemble of pure state trajectories under continuous measurement [4, 5] The stochastic differential equation governing the evolution of the pure state trajectory can be written as

$$d|\psi(t)\rangle = -i\hat{H}_{eff}|\psi(t)\rangle dt + \sum_k \left(\frac{\hat{L}_k|\psi(t)\rangle}{\|\hat{L}_k|\psi(t)\rangle\|} - |\psi(t)\rangle \right) dN_k(t), \quad (6)$$

where the non-Hermitian effective Hamiltonian

$$\hat{H}_{eff} = \hat{H}_s - \frac{i}{2} \sum_k (\hat{L}_k \hat{L}_k^\dagger - \langle \hat{L}_k \hat{L}_k^\dagger \rangle), \quad (7)$$

describes the deterministic evolution of the trajectory. The first term on the right hand side of Eq. 7 is the usual system Hamiltonian, and the non-Hermitian part (terms in bracket) describes the damping process. The terms $\langle \hat{L}_k \hat{L}_k^\dagger \rangle = \langle \psi(t) | \hat{L}_k \hat{L}_k^\dagger | \psi(t) \rangle$ ensure normalization of the wavefunction. The deterministic evolution is interrupted by instantaneous changes to the wavefunction, $|\psi\rangle \rightarrow \frac{\hat{L}_k|\psi\rangle}{\|\hat{L}_k|\psi\rangle\|}$, the so-called quantum jumps described by the second term on the right hand side of Eq. 6. The random numbers $dN_k(t)$ associated to the jumps take on the values of 0 or 1 and have expectation values of

$$E[dN_k(t)] = \langle \psi(t) | \hat{L}_k^\dagger \hat{L}_k | \psi(t) \rangle dt. \quad (8)$$

$E[dN_k(t)]$ represents the probability of a quantum jump associated to the Lindblad operator \hat{L}_k , the total jump probability is thus given by $\sum_k E[dN_k(t)]$.

Next we describe how the stochastic Schrödinger equation can be simulated using variational algorithm described in the main text. We first assume that the wavefunction at time t , $|\psi(t)\rangle$, can be represented by a parametrized ansatz $|\Psi(\theta)\rangle$ prepared in a quantum circuit. Between quantum jumps, the deterministic part of the stochastic Schrödinger can then be simulated with Eqs. 6-8 in the main text, but replacing the system Hamiltonian with the effective Hamiltonian H_{eff} . To realize a quantum jump associated with $\hat{L}_k = \sigma_k^+$, we first note that the raising operator can be written as $\hat{\sigma}_k^+ = e^{-\tau \hat{H}_k} e^{-i\frac{\pi}{2} \hat{\sigma}_k^x}$ for large enough τ [6] and $\hat{H}_k = |0\rangle_k \langle 0|$. Then the quantum jump can be realized in a quantum circuit by evolving the quantum state under σ_k^x for duration $\frac{\pi}{2}$. Then we propagate the state by imaginary time evolution under \hat{H}_k for τ . In our simulations we use $\tau = 20$ and time step of $\delta\tau = 0.01$.

* cheekonglee@tencent.com

- [1] R. Xia and S. Kais, Nat. Commun. **9**, 4195 (2018).
- [2] S. Sorella and L. Capriotti, Physical Review B **61**, 2599 (2000).
- [3] J. R. McClean, S. Boixo, V. N. Smelyanskiy, R. Babbush, and H. Neven, Nature communications **9**, 4812 (2018).
- [4] J. Dalibard, Y. Castin, and K. Mølmer, Physical Review Letters **68**, 580 (1992).
- [5] H. J. Carmichael, Physical Review Letters **70**, 2273 (1993).
- [6] S. Endo, J. Sun, Y. Li, S. C. Benjamin, and X. Yuan, Physical Review Letters **125**, 010501 (2020), arXiv:1812.08778.